



This is a repository copy of *Resonant damping and instability of propagating kink waves in flowing and twisted magnetic flux tubes*.

White Rose Research Online URL for this paper:
<http://eprints.whiterose.ac.uk/162824/>

Version: Published Version

Article:

Bahari, K., Petrukhin, N.S. and Ruderman, M.S. orcid.org/0000-0003-2324-8466 (2020) Resonant damping and instability of propagating kink waves in flowing and twisted magnetic flux tubes. *Monthly Notices of the Royal Astronomical Society*, 496 (1). pp. 67-79. ISSN 0035-8711

<https://doi.org/10.1093/mnras/staa1442>

This article has been accepted for publication in *Monthly Notices of the Royal Astronomical Society* © 2020 The Authors. Published by Oxford University Press on behalf of the Royal Astronomical Society. All rights reserved.

Reuse

Items deposited in White Rose Research Online are protected by copyright, with all rights reserved unless indicated otherwise. They may be downloaded and/or printed for private study, or other acts as permitted by national copyright laws. The publisher or other rights holders may allow further reproduction and re-use of the full text version. This is indicated by the licence information on the White Rose Research Online record for the item.

Takedown

If you consider content in White Rose Research Online to be in breach of UK law, please notify us by emailing eprints@whiterose.ac.uk including the URL of the record and the reason for the withdrawal request.



eprints@whiterose.ac.uk
<https://eprints.whiterose.ac.uk/>

Resonant damping and instability of propagating kink waves in flowing and twisted magnetic flux tubes

K. Bahari¹,¹★ N. S. Petrukhin²★ and M. S. Ruderman^{3,4,5}★

¹Physics Department, Faculty of Science, Razi University, Kermanshah 6714414971, Iran

²Higher School of Economics, National Research University, Moscow 101000, Russia

³School of Mathematics and Statistics (SoMaS), The University of Sheffield, Hicks Building, Hounsfield Road, Sheffield S3 7RH, UK

⁴Department of Planetary Physics, Space Research Institute, Russian Academy of Sciences (IKI), Moscow 117997, Russia

⁵Moscow Center for Fundamental and Applied Mathematics, Lomonosov Moscow State University, GSP-1, Leninskie Gory, Moscow, 119991, Russia

Accepted 2020 May 20. Received 2020 May 9; in original form 2020 March 21

ABSTRACT

We study the propagation and stability of kink waves in a twisted magnetic tube with the flow. The flow velocity is assumed to be parallel to the magnetic field, and the magnetic field lines are straight outside the tube. The density is constant inside and outside of the tube, and it monotonically decreases from its value inside the tube to that outside in the transitional or boundary layer. The flow speed and magnetic twist monotonically decrease in the transitional layer from their values inside the tube to zero outside. Using the thin tube and thin boundary layer (TTTB) approximation, we derived the dispersion equation determining the dependence of the wave frequency and decrement/increment on the wavenumber. When the kink wave frequency coincides with the local Alfvén frequency at a resonant surface inside the transitional layer, the kink wave is subjected to either resonant damping or resonant instability. We study the properties of kink waves in a particular unperturbed state where there is no flow and magnetic twist in the transitional layer. It is shown that in a tube with flow, the kink waves can propagate without damping for particular values of the flow speed. Kink waves propagating in the flow direction either damp or propagate without damping. Waves propagating in the opposite direction can either propagate without damping, or damp, or become unstable. The theoretical results are applied to the problem of excitation of kink waves in spicules and filaments in the solar atmosphere.

Key words: MHD – plasmas – waves – Sun: corona – Sun: oscillations .

1 INTRODUCTION

Kink oscillations of magnetic flux tubes were first observed in the solar atmosphere by the *Transition Region and Coronal Explorer* (TRACE) mission in 1998 and reported by Aschwanden et al. (1999) and Nakariakov et al. (1999). They were transverse oscillations of coronal magnetic loops. Later, similar oscillations were observed in prominence fibrils (e.g. Hillier et al. 2013; Arregui 2018). All these oscillations were standing kink waves.

Propagating kink waves in solar magnetic flux tubes were also observed. They were observed in coronal magnetic loops (Tomczyk et al. 2007; Tomczyk & McIntosh 2009; Pascoe, Wright & De Moortel 2010), in spicules (De Pontieu et al. 2007; He et al. 2009a,b), in the fine structure of prominences (Okamoto et al. 2007), in soft X-ray coronal jets (Cirtain et al. 2007; Vasheghani Farahani

et al. 2009), in filament threads (Lin et al. 2007, 2009), and in chromospheric mottles (Kuridze et al. 2012). Morton et al. (2012) reported the observations of simultaneous propagation of kink and sausage waves in a range of chromospheric magnetic wave guides.

The first theoretical study of kink waves in magnetic flux tubes were carried out by Ryutov & Ryutova (1976). In particular, these authors obtained the expression for the phase speed of kink waves in the thin tube approximation. Ryutov & Ryutova (1976) considered a magnetic tube with straight magnetic field lines. Later, kink waves in more sophisticated models of magnetic tubes were studied (see e.g. the review by Ruderman & Erdélyi 2009). One particular property of magnetic flux tubes that can affect the kink waves is magnetic twist. The effect of magnetic twist both on propagating (Bennet, Roberts & Narain 1999; Carter & Erdélyi 2007, 2008; Ruderman 2015; Bahari & Khalvandi 2017) as well as on standing (Ruderman 2007; Erdélyi & Fedun 2010; Karami & Bahari 2012; Terradas & Goossens 2012; Ruderman & Terradas 2015) kink oscillations in solar magnetic flux tubes was studied.

* E-mail: karam.bahari@gmail.com (KB); npetruhin@hse.ru (NSP); M.S.Ruderman@sheffield.ac.uk (MSR)

Another important property of magnetic flux tubes in the solar atmosphere is the almost ubiquitous presence of plasma flows. They were observed in active regions (Brekke, Kjeldseth-Moe & Harrison 1997; Winebarger, DeLuca & Golub 2001; Winebarger et al. 2002; Teriaca et al. 2004; Doyle et al. 2006; Ofman & Wang 2008; Tian et al. 2008, 2009), in prominence threads (Chae et al. 2008; Terradas et al. 2008), and solar atmospheric jets (Shibata et al. 2007; Nishizuka et al. 2011; see also the review by Raouafi et al. 2016). The effect of flow on kink waves in magnetic flux tubes was studied by many authors (e.g. Terra-Homem, Erdélyi & Ballai 2003; Ruderman 2010; Soler & Goossens 2011; Terradas et al. 2011; Bahari 2017).

Already, the first observation of standing kink oscillations revealed that they are strongly damped with the damping time of the order of a few oscillation periods (Nakariakov et al. 1999). At present, it is almost generally accepted in the solar physics that this damping is caused by resonance absorption. To our knowledge, Ionson (1978) was the first who pointed out the importance of resonance absorption for wave processes in the solar atmosphere. Since then resonant absorption remained a popular mechanism for explaining various solar phenomena, especially wave damping. Hollweg & Yang (1988) studied resonant damping of surface waves in a thin transitional layer sandwiched with two semi-infinite regions with cold homogeneous plasmas and constant magnetic field in the whole space. Considering the limiting case of surface waves propagating almost perpendicular to the magnetic field, they managed to obtain the expression for the damping rate of kink waves propagating in a thin magnetic flux tube. Goossens, Hollweg & Sakurai (1992) derived the general expression for the decrement of kink waves propagating in a twisted magnetic tube.

Studies of resonant damping of kink waves in solar magnetic wave guides received a new impetus after the first observation of damped kink oscillations of coronal magnetic loops. Ruderman & Roberts (2002) and Goossens, Andries & Aschwanden (2002) showed how the observed damping of these oscillations can be used in coronal seismology (see also the reviews by Andries et al. 2009; Ruderman & Erdélyi 2009). To-date resonant damping of kink waves in magnetic flux tubes have been studied in a variety of equilibria, including twisted and expanded tubes, and in the presence of flow (see the review by Goossens, Erdélyi & Ruderman 2011, and recent articles by Shukhobodskiy & Ruderman 2018; Ebrahimi & Bahari 2019; Ruderman & Petrukhin 2019).

Resonant absorption was considered as a course of wave damping. However, the presence of background balk flow can result in a new phenomenon called resonant instability. It is intrinsically related to the presence of negative energy waves. The theory of negative energy waves can be found in the reviews by Nezhlin (1976), Ostrovskii, Rybak & Tsimring (1986), and Stepanyants & Fabrikant (1989), and in the book by Fabrikant & Stepanyants (1998). To our knowledge the application of the theory of negative energy waves to waves in magnetic flux tubes was first discussed by Ryutova (1988). Resonant instability is a particular case of negative energy wave instability when the decrease in the wave energy is caused by resonant absorption. Its main property is that this instability occurs for the values of flow speed below that needed to cause the KH instability. The resonant instability was studied in the framework of magneto-hydrodynamics (MHD) by many authors (e.g. Ruderman & Wright 1998; Tirry et al. 1998; Erdélyi & Taroyan 2003; Ruderman & Belov 2010; Taroyan & Ruderman 2011). This concept was also applied to solar physics. Andries & Goossens (2001) studied resonant flow instabilities in coronal plumes. However, in general, the concept

of resonant instability did not receive much attention in solar physics.

In this paper, we now consider a problem similar to one studied by Bahari (2018). However, Bahari (2018) used the approximation of incompressible plasma, while here we use the approximation of cold plasma that is more relevant for applications to studying kink waves in the solar atmosphere. Also, Bahari (2018) only studied the wave damping, while here we also investigate the resonant instability.

This paper is organized as follows. In the next section, we formulate the problem and describe the unperturbed state. In Section 3, we derive the dispersion equation determining the dependence of the wave frequency and decrement/increment on the wavenumber. In Section 4, we obtain the approximate solution to the dispersion equation using the regular perturbation method with the ratio of the thickness of the transitional layer to the tube radius as a small parameter. In Section 5, we obtain the expression for the decrement/increment of propagating kink waves for a particular unperturbed state. In Section 6, we apply the theoretical results to the problem of kink wave excitation in spicules and filaments in the solar atmosphere. Section 7 contains the summary of the obtained results and our conclusions.

2 PROBLEM FORMULATION AND UNPERTURBED STATE

We consider a twisted magnetic tube with a background equilibrium flow and use the cold plasma approximation. In cylindrical coordinates r, ϕ, z , the unperturbed magnetic field and flow velocity are given by $\mathbf{B} = (0, B_\phi(r), B_z(r))$, and $\mathbf{U} = (0, U_\phi(r), U_z(r))$, respectively. The equilibrium density is given by

$$\rho = \begin{cases} \rho_i, & r \leq R(1 - l/2), \\ \rho_i(r), & R(1 - l/2) \leq r \leq R(1 + l/2), \\ \rho_e, & r \geq R(1 + l/2), \end{cases} \quad (1)$$

where ρ_i and ρ_e are constants, $\rho_e < \rho_i$, $\rho_i(r)$ is a monotonically decreasing function, and ρ is continuous at $r = R(1 \pm l/2)$. The domain defined by $r \leq R(1 - l/2)$ is the core part of the magnetic tube, while $R(1 - l/2) \leq r \leq R(1 + l/2)$ is the transitional region. It is assumed that there is no plasma flow outside of the tube, that is $\mathbf{U} = 0$ for $r \geq R(1 + l/2)$. The azimuthal components of the magnetic field and velocity are given by

$$B_\phi = \begin{cases} Ar, & r \leq R(1 - l/2), \\ B_{\phi t}(r), & R(1 - l/2) \leq r \leq R(1 + l/2), \\ 0, & r \geq R(1 + l/2), \end{cases} \quad (2)$$

$$U_\phi = \begin{cases} Vr, & r \leq R(1 - l/2), \\ U_{\phi t}(r), & R(1 - l/2) \leq r \leq R(1 + l/2), \\ 0, & r \geq R(1 + l/2). \end{cases} \quad (3)$$

It is assumed that both $B_{\phi t}$ and $U_{\phi t}$ are continuous and monotonically decreasing functions. When there is no flow and transitional layer (i.e. $\mathbf{U} = 0$ and $l = 0$), the equilibrium magnetic field coincides with that used by Ruderman (2007).

The magnetic field and velocity are related by the momentum equation

$$\frac{d}{dr} (B_\phi^2 + B_z^2) = \frac{2}{r} (\mu_0 \rho U_\phi^2 - B_\phi^2). \quad (4)$$

In particular, it follows from this equation that the z -component of the magnetic field is constant outside of the tube, $B_z = B_0 = \text{constant}$ for $r \geq R(1 + l/2)$.

A popular unperturbed state is the one with twisted magnetic tube but with a purely axial velocity inside the tube. Such an unperturbed state was, for example, used when studying the KH instability (e.g. Zhelyazkov & Zaqarashvili 2012; Zaqarashvili, Vörös & Zhelyazkov 2014; Zhelyazkov 2015). In this unperturbed state, plasma flows across the magnetic field lines. As a result, there is the electrical field equal to $-\mathbf{U} \times \mathbf{B}$, which, for typical parameters of various jets in the solar atmosphere, should be quite strong. This electrical field drives the electrical current, and the related Joule dissipation can result in quick damping of the velocity component orthogonal to the magnetic field. Hence, it looks like a viable assumption that the plasma flows along the magnetic field lines. In accordance with this, we now make the same assumption as in Cheremnykh et al. (2018) and Bahari (2018), namely that the velocity is parallel to the magnetic field, $\mathbf{U} \parallel \mathbf{B}$. This assumption implies that

$$\frac{U_\phi}{U_z} = \frac{B_\phi}{B_z}. \quad (5)$$

We even can speculate that this relation can explain the observed rotation of various kinds of jets in the solar atmosphere (e.g. Liu et al. 2009, 2011; Kamio et al. 2010; Zhang & Ji 2014). The jet rotation is established on the basis of observation of the azimuthal velocity component. When the plasma moves along twisted magnetic field lines, this velocity component is naturally present.

It follows from equations (4) and (5) that the z -components of magnetic field and velocity, in the core region ($r \leq R(1 - l/2)$), are defined by

$$\begin{aligned} B_z^2 &= B_1^2 + r^2 (\mu_0 \rho_1 V^2 - 2A^2), \\ U_z^2 &= \frac{V^2}{A^2} [B_1^2 + r^2 (\mu_0 \rho_1 V^2 - 2A^2)], \end{aligned} \quad (6)$$

where B_1 is a positive constant. We also obtain from equation (4) and the continuity of the magnetic field at the external boundary of the transition region that

$$\begin{aligned} B_{z1}^2(r) &= B_0^2 - B_{\phi t}^2(r) \\ &+ 2 \int_r^{R(1+l/2)} [\mu_0 \rho(\tilde{r}) U_{\phi t}^2(\tilde{r}) - B_{\phi t}^2(\tilde{r})] \frac{d\tilde{r}}{\tilde{r}}. \end{aligned} \quad (7)$$

The condition that B_z is continuous at the internal boundary of the transitional layer yields

$$\begin{aligned} B_1^2 + R^2(1 - l/2)^2 (\mu_0 \rho_1 V^2 - 2A^2) + B_{\phi t}^2(R(1 - l/2)) \\ = B_0^2 + 2 \int_{R(1-l/2)}^{R(1+l/2)} [\mu_0 \rho(r) U_{\phi t}^2(r) - B_{\phi t}^2(r)] \frac{dr}{r}. \end{aligned} \quad (8)$$

Finally, it follows from equation (5) that the ϕ -component of the velocity in the transitional layer is defined by

$$U_{\phi t}(r) = B_{\phi t}(r) \frac{U_{z1}(r)}{B_{z1}(r)}. \quad (9)$$

We can always choose the direction of the z -axis in such a way that $U_z(r) > 0$. Since the MHD equations are invariant with respect to the change of sign of the magnetic field, we can assume that $B_z(r) > 0$. Then, it follows from equation (9) and the continuity of the equilibrium velocity and magnetic field that $U_\phi(r)$ and $B_\phi(r)$ have the same signs.

At present, the only condition imposed on $B_{\phi t}(r)$ and $U_{\phi t}(r)$ is that these are monotonic functions. We note that the unperturbed state considered in this paper is the same as the one used by Bahari (2018).

To describe the plasma motion, we use the linear MHD equations in the cold plasma approximation. We introduce the characteristic wavelength λ and assume that $R/\lambda = \epsilon \ll 1$, meaning that we use the long wavelength or thin tube approximation. We also assume that the thickness of the transitional or boundary layer is lR with $l \ll 1$ meaning that we use the thin boundary approximation. Summarizing, we use the thin tube and thin boundary layer (TTTB) approximation. In addition, we assume that magnetic field lines make no more than a few turns on one wavelength. This implies that B_ϕ/B_z is of the order of ϵ . Then, it follows from equation (5) that U_ϕ/U_z is also of the order of ϵ . In accordance with this, we write

$$A = \epsilon \tilde{A}, \quad B_{\phi t} = \epsilon \tilde{B}_{\phi t}, \quad V = \epsilon \tilde{V}, \quad U_{\phi t} = \epsilon \tilde{U}_{\phi t}, \quad (10)$$

where \tilde{A} is of the order of $B_0 R^{-1}$, $\tilde{B}_{\phi t}$ is of the order of B_0 , \tilde{V} is of the order of $U_z R^{-1}$, and $\tilde{U}_{\phi t}$ is of the order of U_z . Hence, in equation (10), the quantities without tildes are of the order of ϵ , while the quantities with tildes are of the order of unity. Now, it follows from equations (6)–(8) that

$$B_1 = B_0 + \mathcal{O}(\epsilon^2), \quad B_z = B_0 + \mathcal{O}(\epsilon^2) \quad (11)$$

everywhere, and

$$U_z = \frac{V}{A} B_0 \equiv U_0 + \mathcal{O}(\epsilon^2) \quad (12)$$

in the core region. Hence, we consider the equilibrium with almost constant axial magnetic field and weak azimuthal field. The same is true for the flow in the core region.

3 DERIVATION OF THE DISPERSION EQUATION

We consider propagating kink waves. To describe these waves, we use the linearized MHD equations in the cold plasma approximation. We use the ideal MHD equations everywhere but in the dissipative layer embracing an ideal resonant surface. Since the unperturbed state is independent of ϕ and z , we can Fourier-analyse perturbations of all variables with respect to these two coordinates. In addition, we only consider the solutions in the form of normal modes. We take the perturbations of all variables proportional to $\exp[i(-\omega t + m\phi + kz)]$, where $m = \pm 1$, k is real, and ω is complex. Goossens et al. (1992) (hereafter Paper I) showed that after that the ideal MHD equations can be reduced to the system of two equations for the perturbation of the magnetic pressure P and the radial component of the plasma displacement ξ_r . In Paper I, a finite-beta plasma was considered. Since we use the cold plasma approximation, we take the plasma pressure perturbation and the sound speed equal to zero in the equations derived in Paper I. As a result, we obtain

$$D \frac{d(r\xi_r)}{dr} = C_1 r \xi_r - C_2 r P, \quad (13)$$

$$D \frac{dP}{dr} = C_3 \xi_r - C_1 P. \quad (14)$$

In these equations, the following notations are used:

$$V_A^2 = \frac{B^2}{\mu_0 \rho}, \quad \mathbf{k} = \left(0, \frac{m}{r}, k\right), \quad (15)$$

$$f_B = \mathbf{k} \cdot \mathbf{B} = \frac{m}{r} B_\phi + k B_z, \quad \omega_A^2 = \frac{f_B^2}{\mu_0 \rho}, \quad (16)$$

$$\omega_f = \mathbf{k} \cdot \mathbf{U} = \frac{m}{r} U_\phi + k U_z, \quad \Omega = \omega - \omega_f, \quad (17)$$

$$T = \frac{f_B B_\phi}{\mu_0} + \rho \Omega U_\phi, \quad (18)$$

$$Q = \frac{2\Omega^2 B_\phi^2}{\mu_0 r} + \frac{2\Omega f_B B_\phi U_\phi}{\mu_0 r} - \frac{\rho U_\phi^2}{r} (\Omega^2 - \omega_A^2), \quad (19)$$

$$D = \rho V_A^2 \Omega^2 (\Omega^2 - \omega_A^2), \quad C_1 = \Omega^2 \left(Q - \frac{2m}{r^2} V_A^2 T \right), \quad (20)$$

$$C_2 = \Omega^2 \left[\Omega^2 - V_A^2 \left(k^2 + \frac{1}{r^2} \right) \right], \quad (21)$$

$$C_3 = D \left\{ r \frac{d}{dr} \left[\frac{1}{\mu_0} \left(\frac{B_\phi}{r} \right)^2 - \rho \left(\frac{U_\phi}{r} \right)^2 \right] + \rho (\Omega^2 - \omega_A^2) \right\} + Q^2 - \frac{4}{r^2} V_A^2 \Omega^2 T^2. \quad (22)$$

We emphasize that the system of equations (13) and (14) can only be used far from dissipative layers, where we can neglect dissipation. We note that, although $|B_\phi| \ll B_z$, the contributions of the axial and azimuthal field in the Alfvén frequency ω_A are of the same order. In the core region, the ratio of these contributions is of the order of $\lambda|A|/B_0 = \mathcal{O}(1)$. Since the axial magnetic field is almost constant everywhere while the azimuthal field monotonically decreases in the transitional layer, this ratio also decreases monotonically in this layer and becomes zero at its external boundary. The same is true for the ratio of contributions of U_ϕ and U_z in ω_f .

While the Alfvén frequency ω_A and the frequency ω_f defining the Doppler shift are constant in the core region and outside the tube, they vary in the transitional layer. This variation is very important because it defines the Alfvén continuum responsible for resonant damping or resonant instability. Let us now consider an example. We assume that the density is a linear function of r inside the transitional layer given by

$$\rho_i(r) = \frac{\rho_i + \rho_e}{2} + \frac{(\rho_i - \rho_e)(R - r)}{lR}. \quad (23)$$

We also assume that B_ϕ and U_z are given in the transitional layer by

$$B_{\phi i}(r) = \begin{cases} \frac{Ar}{l\theta} \left(2 - \frac{2r}{R} - l + l\theta \right), & R(1 - l/2) \leq r \leq r_a, \\ 0, & r > r_a, \end{cases} \quad (24)$$

$$U_{zi}(r) = \begin{cases} \frac{U_0}{l\theta} \left(2 - \frac{2r}{R} - l + l\theta \right), & R(1 - l/2) \leq r \leq r_a, \\ 0, & r > r_a, \end{cases} \quad (25)$$

where $\theta \leq 2$ and $r_a = R[1 - l(1 - \theta)/2]$. The azimuthal velocity $U_{\phi i}(r)$ is defined by equation (5). Using this equation, and equations (24) and (25), we obtain

$$U_{\phi i}(r) = \begin{cases} \frac{AU_0 r}{B_0 l^2 \theta^2} \left(2 - \frac{2r}{R} - l + l\theta \right)^2, & R(1 - l/2) \leq r \leq r_a, \\ 0, & r > r_a. \end{cases} \quad (26)$$

This equilibrium is similar to the one considered by Ruderman & Petrukhin (2019).

For this equilibrium, we calculated the Alfvén frequency ω_A and the frequencies

$$\omega_{D\pm} = \omega_f \pm \omega_A \quad (27)$$

that define the Doppler-shifted Alfvén continuum. In Figs 1 and 2, the dependences of ω_A and $\omega_{D\pm}$ on the dimensionless distance

$$x = \frac{r - R(1 - l/2)}{lR} \quad (28)$$

are shown for $\theta = 2$, $M_A = 1$, $\zeta = 10$, and $A = kB_0$, where the Alfvén Mach number M_A , Alfvén speed in the core region V_{Ai} , and

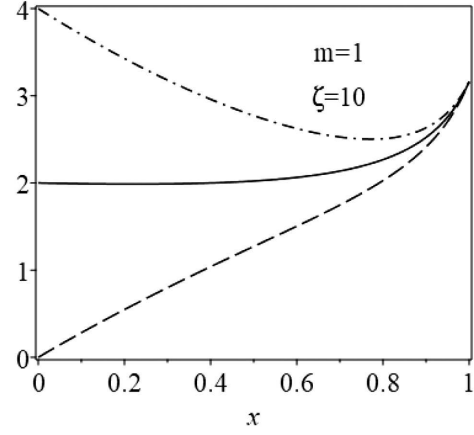


Figure 1. Dependence of frequencies on x for $m = 1$ and $\zeta = 10$. The solid, dashed, and dash-dotted curves correspond to ω_A , ω_{D-} , and ω_{D+} , respectively.

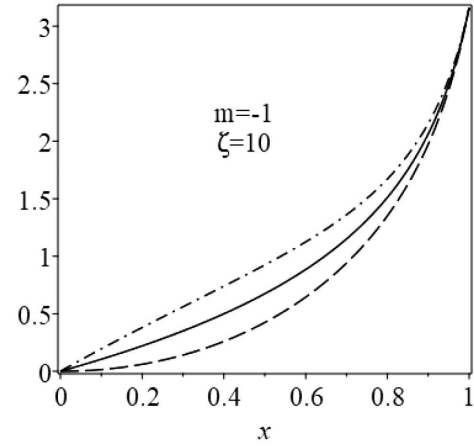


Figure 2. Dependence of frequencies on x for $m = -1$ and $\zeta = 10$. The solid, dashed, and dash-dotted curves correspond to ω_A , ω_{D-} , and ω_{D+} , respectively.

the ratio of densities ζ are defined by

$$M_A = \frac{U_0}{V_{Ai}}, \quad V_{Ai} = \frac{B_0}{\sqrt{\mu_0 \rho_i}}, \quad \zeta = \frac{\rho_i}{\rho_e}. \quad (29)$$

The relation $A = kB_0$ indicates that each magnetic field line in the core region makes one full turn about the z -axis for a wavelength. We take the maximum possible value of $\theta = 2$ because, for $\theta < 2$, the graphs of ω_A and ω_{D+} would overlap in the interval $[\theta/2, 1]$.

The Alfvén continuum consists of two intervals,

$$[-\omega_{Ae}, -\omega_{Ai}] \cup [\omega_{Ai}, \omega_{Ae}]. \quad (30)$$

The Doppler-shifted Alfvén continuum is also the union of two intervals

$$[\min \omega_{D-}, \max \omega_{D-}] \cup [\min \omega_{D+}, \max \omega_{D+}]. \quad (31)$$

For particular values of parameters, we choose to calculate ω_A and $\omega_{D\pm}$, we obtain that $\max \omega_{D-} > \min \omega_{D+}$ when $m = 1$. Therefore, the Doppler-shifted Alfvén continuum is $[\min \omega_{D-}, \max \omega_{D+}]$. For $m = -1$, we have

$$\omega_{Ai} = \min \omega_{D-} = \min \omega_{D+} = 0,$$

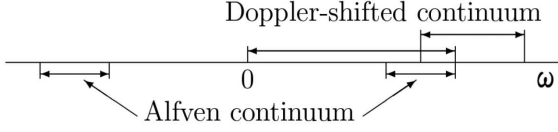


Figure 3. Schematic picture of the Alfvén and Doppler-shifted Alfvén continua for $m = 1$.

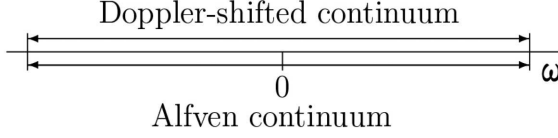


Figure 4. Schematic picture of the Alfvén and Doppler-shifted Alfvén continua for $m = -1$.

$$\max \omega_{D-} = \max \omega_{D+} = \omega_{Ae}.$$

In this latter case, the Doppler-shifted Alfvén continuum coincides with the Alfvén continuum, which consists of the interval $[-\omega_{Ae}, \omega_{Ae}]$. The Alfvén continuum and the Doppler-shifted Alfvén continua are schematically shown in Fig. 3 for $m = 1$ and in Fig. 4 for $m = -1$.

We introduce the parallel and perpendicular components of the plasma displacement

$$\xi_{\parallel} = \frac{\mathbf{B} \cdot \boldsymbol{\xi}}{B}, \quad \xi_{\perp} = \frac{1}{B} (\xi_{\phi} B_z - \xi_z B_{\phi}). \quad (32)$$

The expressions for ξ_{\parallel} and ξ_{\perp} in terms of ξ_r and P were derived in Paper I. In the cold plasma approximation, they reduce to

$$\Omega^2 \xi_{\parallel} = -\frac{i \xi_r U_{\phi}}{r B} (2\Omega B_{\phi} + f_B U_{\phi}), \quad (33)$$

$$(\Omega^2 - \omega_A^2) \xi_{\perp} = \frac{i}{\rho r B} (r g_B P - 2B_z T \xi_r), \quad (34)$$

where

$$g_B = \frac{m}{r} B_z - k B_{\phi}. \quad (35)$$

The only fixed spatial scale in the problem is the tube radius R . We take the Alfvén speed in the tube core, V_{Ai} , as the characteristic velocity of the problem. Then, the fixed frequency is V_{Ai}/R . We consider long waves with the characteristic wavelength $\lambda = \epsilon^{-1}R$, as we have already stated this earlier. This implies that the characteristic axial wavenumber of the waves is ϵ/R , and the characteristic frequency is $\epsilon V_{Ai}/R$. In accordance with this, we now introduce the scaled frequency and wavenumber

$$\omega = \epsilon \varpi, \quad k = \epsilon \kappa. \quad (36)$$

Using equations (10), (13), (20), and (21), we obtain the estimate $P/\rho V_A^2 \sim \epsilon^2 \xi_r/R$. Hence, we obtained a well-known result that P is proportional to $\epsilon^2 = (R/\lambda)^2$ (see e.g. Goossens et al. 2009). In accordance with this, we introduce the scaled magnetic pressure perturbation $P = \epsilon^2 \tilde{P}$. Then, in the leading-order approximation with respect to ϵ equations (13) and (14) reduce to

$$\rho(\tilde{\Omega}^2 - \omega_A^2) \frac{d(r \xi_r)}{dr} = \frac{1}{r} \tilde{P} - \frac{2m}{r} \tilde{T} \xi_r, \quad (37)$$

$$\rho(\tilde{\Omega}^2 - \omega_A^2) \frac{d\tilde{P}}{dr} = W \xi_r + \frac{2m}{r^2} \tilde{T} \tilde{P}, \quad (38)$$

where

$$\tilde{f}_B = \frac{m}{r} \tilde{B}_{\phi} + \kappa B_0, \quad \omega_A^2 = \frac{\tilde{f}_B^2}{\mu_0 \rho}, \quad \tilde{\Omega} = \varpi - \varpi_f, \quad (39)$$

$$\varpi_f = \frac{m}{r} \tilde{U}_{\phi} + \kappa U_z, \quad \tilde{T} = \frac{\tilde{f}_B \tilde{B}_{\phi}}{\mu_0} + \rho \tilde{\Omega} \tilde{U}_{\phi}, \quad (40)$$

$$W = \rho(\tilde{\Omega}^2 - \omega_A^2) \left[r \frac{d\Psi}{dr} + \rho(\tilde{\Omega}^2 - \omega_A^2) \right] - \frac{4}{r^2} \tilde{T}^2, \quad (41)$$

$$\Psi = \frac{1}{\mu_0} \left(\frac{\tilde{B}_{\phi}}{r} \right)^2 - \rho \left(\frac{\tilde{U}_{\phi}}{r} \right)^2. \quad (42)$$

Now, we look for the solution separately in the core region, in the surrounding plasma, and in the transitional layer.

3.1 Solution in the core region

Using equations (2), (3), and (11), we obtain

$$\tilde{f}_B = m \tilde{A} + \kappa B_0, \quad \varpi_f = m \tilde{V} + \kappa U_0, \quad (43)$$

while equations (13) and (14) reduce to

$$\rho_i(\tilde{\Omega}^2 - \omega_{Ai}^2) \frac{d(r \xi_r)}{dr} = \frac{1}{r} \tilde{P} - 2m \bar{T} \xi_r, \quad (44)$$

$$\rho_i(\tilde{\Omega}^2 - \omega_{Ai}^2) \frac{d\tilde{P}}{dr} = \bar{W}_i \xi_r + \frac{2m}{r} \bar{T} \tilde{P}, \quad (45)$$

where

$$\bar{T} = \frac{\tilde{T}}{r} = \frac{\tilde{f}_B \tilde{A}}{\mu_0} + \rho_i \tilde{\Omega} \tilde{V}, \quad (46)$$

$$\bar{W}_i = \rho_i^2 (\tilde{\Omega}^2 - \omega_{Ai}^2)^2 - 4\bar{T}^2. \quad (47)$$

Eliminating \tilde{P} from equations (44) and (45) yields

$$\frac{d}{dr} r \frac{d(r \xi_r)}{dr} - \xi_r = 0. \quad (48)$$

It follows from this equation and the condition that ξ_r must be regular at $r = 0$ that $\xi_r = \text{constant}$, that is the radial plasma displacement is independent of r in the core region. Previously, this result was explicitly stated by Goossens et al. (2009) for an untwisted tube. Later, it was obtained for a twisted tube by Ruderman (2015). Hence, neither the magnetic twist nor the flow affect the result that ξ_r is constant inside the tube in the thin tube approximation. It is convenient to introduce the special notation for ξ_r in the core region. Below, we denote it as η . Now, we obtain from equation (44)

$$\tilde{P} = r \eta [\rho_i (\tilde{\Omega}^2 - \omega_{Ai}^2) + 2m \bar{T}]. \quad (49)$$

3.2 Solution outside the tube

Recall that $U = 0$ and $B_{\phi} = 0$ for $r \geq R(1 + l/2)$. Then, we obtain outside the tube

$$\tilde{f}_B = \kappa B_0, \quad \varpi_f = 0, \quad \tilde{T} = 0, \quad (50)$$

$$W = \rho_e^2 (\varpi^2 - \omega_{Ae}^2)^2. \quad (51)$$

Equations (37) and (38) reduce to

$$\rho_e (\varpi^2 - \omega_{Ae}^2) \frac{d(r \xi_r)}{dr} = \frac{1}{r} \tilde{P}, \quad (52)$$

$$\frac{d\tilde{P}}{dr} = \rho_e (\varpi^2 - \omega_{Ae}^2) \xi_r. \quad (53)$$

Eliminating \tilde{P} from these equations, we obtain

$$\frac{d}{dr} r^3 \frac{d\xi_r}{dr} = 0. \quad (54)$$

Taking into account that $\xi_r \rightarrow 0$ as $r \rightarrow \infty$, we obtain from this equation

$$\xi_r = \frac{\psi}{r^2}, \quad (55)$$

where ψ is a constant. Substituting this expression in equation (52) yields

$$\tilde{P} = -\rho_e (\varpi^2 - \varpi_{\text{Ae}}^2) \frac{\psi}{r}. \quad (56)$$

The dependences of ξ_r , \tilde{P} , and also ξ_ϕ on r , in the case when there is no transitional layer ($l = 0$), are shown in Fig. 1 in Goossens et al. (2009).

3.3 Solution in the transitional layer

In this section, we obtain the solution in the transitional layer. We will see below that for some wave modes there is a resonant surface inside the transitional layer, where $\tilde{\Omega}^2 = \varpi_{\text{A}}^2$. The position of this surface is defined by $r = r_{\text{A}}, R(1 - 1/2) < r_{\text{A}} < R(1 + 1/2)$. When ϖ is real, the solution has a singularity at this surface. Small imaginary part of ϖ removes this singularity, however, still there are large gradients in the vicinity of resonant surface. This implies that, in this vicinity the dissipation is important. This observation suggests the method for solving the problem. We solve the dissipative MHD equations in the vicinity of the resonant surface and the ideal MHD equations far from the resonant surface. Then, we match the solutions in the two overlap regions at the two sides of the resonant surface, where both ideal and dissipative solutions are valid (e.g. Goossens & Ruderman 1995; Goossens et al. 2011).

3.3.1 Ideal solution far from the resonant surface

The expression for W given by equations (41) contains the derivative with respect to r . Because of this term, the variation of \tilde{P} across the transitional layer is of the order of \tilde{P} , which makes it difficult to solve the system of equations (37) and (38) in the transitional layer. To resolve this problem, we introduce the new variable

$$\hat{P} = \tilde{P} - r \xi_r \Psi. \quad (57)$$

Using this variable substitution, we transform equations (37) and (38) into

$$\rho (\tilde{\Omega}^2 - \varpi_{\text{A}}^2) \frac{d(r \xi_r)}{dr} = \frac{1}{r} \hat{P} + \left(\Psi - \frac{2m}{r} \tilde{T} \right) \xi_r, \quad (58)$$

$$\rho (\tilde{\Omega}^2 - \varpi_{\text{A}}^2) \frac{d\hat{P}}{dr} = \left[\rho^2 (\tilde{\Omega}^2 - \varpi_{\text{A}}^2)^2 - \left(\Psi - \frac{2m}{r} \tilde{T} \right)^2 \right] \xi_r + \left(\frac{2m}{r^2} \tilde{T} - \frac{\Psi}{r} \right) \hat{P}. \quad (59)$$

We need to calculate ξ_r and \hat{P} with accuracy up to the terms of the order of l . The characteristic scale of variation of these quantities in the transitional layer is lR . This implies that in equations (58) and (59), we can calculate the right-hand sides in the leading-order approximation with respect to l , that is, we can neglect terms of the order of l and of the higher order. In particular, we can substitute ϖ_r for ϖ and R for $R(1 \pm 1/2)$. In addition, the variations of ξ_r and \hat{P} are of the order of l in the transitional layer. This implies that we

can substitute the values of these quantities at $r = R(1 - l/2)$ when calculating the variations of ξ_r and \hat{P} across the transitional layer. Now, using equations (2), (3), (12), (43), (46), and (57), we obtain that the solution to equations (58) and (59) is given by

$$\xi_r = \eta + \frac{\eta}{R} \int_{R(1-1/2)}^r \frac{X dr'}{\rho_t (\tilde{\Omega}_r^2 - \varpi_{\text{A}}^2)}, \quad (60)$$

$$\hat{P} = \eta \rho_i R(1 - l/2) [(\varpi - \kappa U_0)^2 - \kappa^2 V_{\text{Ai}}^2] + \eta \int_{R(1-1/2)}^r \left(\rho_t (\tilde{\Omega}^2 - \varpi_{\text{Ai}}^2) + \frac{Y}{\rho_t (\tilde{\Omega}_r^2 - \varpi_{\text{Ai}}^2)} \right) dr', \quad (61)$$

for $R(1 - l/2) \leq r < r_{\text{A}}$, and by

$$\xi_r = \frac{\psi}{R^2(1+l)} - \frac{\eta}{R} \int_r^{R(1+1/2)} \frac{X dr'}{\rho_t (\tilde{\Omega}_r^2 - \varpi_{\text{A}}^2)}, \quad (62)$$

$$\hat{P} = -\frac{\psi \rho_e (\varpi^2 - \varpi_{\text{Ae}}^2)}{R(1+l/2)} - \eta \int_r^{R(1+1/2)} \left(\rho_t (\tilde{\Omega}^2 - \varpi_{\text{A}}^2) + \frac{Y}{\rho_t (\tilde{\Omega}_r^2 - \varpi_{\text{A}}^2)} \right) dr', \quad (63)$$

for $r_{\text{A}} < r \leq R(1 + l/2)$, where $\tilde{\Omega}_r$ is the real part of $\tilde{\Omega}$,

$$X = \rho_i [(\varpi - \kappa U_0)^2 - \kappa^2 V_{\text{Ai}}^2] + \Psi - 2m\tilde{T}/R, \quad (64)$$

$$Y = \rho_i \left(\frac{2m}{R} \tilde{T} - \Psi \right) \left[(\varpi - \kappa U_0)^2 - \kappa^2 V_{\text{Ai}}^2 - \frac{2m}{R} \tilde{T} + \Psi \right]. \quad (65)$$

Using equations (57) and (60)–(63), we obtain that the pressure perturbation is given by

$$\tilde{P} = \eta \rho_i R(1 - l/2) [(\varpi - \kappa U_0)^2 - \kappa^2 V_{\text{Ai}}^2] + \eta r \Psi(r) + \eta \int_{R(1-1/2)}^r \left(\rho_t (\tilde{\Omega}^2 - \varpi_{\text{A}}^2) + \frac{Y(r') + \Psi(r)X(r')}{\rho_t (\tilde{\Omega}_r^2 - \varpi_{\text{A}}^2)} \right) dr', \quad (66)$$

for $R(1 - l/2) \leq r < r_{\text{A}}$, and by

$$\tilde{P} = -\frac{\psi \rho_e (\varpi^2 - \varpi_{\text{Ae}}^2)}{R(1+l/2)} + \eta r \Psi(r) - \eta \int_r^{R(1+1/2)} \left(\rho_t (\tilde{\Omega}^2 - \varpi_{\text{A}}^2) + \frac{Y(r') + \Psi(r)X(r')}{\rho_t (\tilde{\Omega}_r^2 - \varpi_{\text{A}}^2)} \right) dr', \quad (67)$$

for $r_{\text{A}} < r \leq R(1 + l/2)$. We emphasize that the expressions for ξ_r and \tilde{P} are only valid not too close to the resonant surface. Therefore, the inequalities $r < r_{\text{A}}$ and $r > r_{\text{A}}$ only indicate that a corresponding expression is valid either at the left or right of the resonant surface, but they do not mean that this expression is valid for r arbitrarily close to r_{A} . The condition ‘not too close to the resonant surface’ will be specified in the next subsection.

3.3.2 Dissipative solution near the resonant surface

In principle, we can avoid finding the solution in the dissipative layer and use the connection formulae derived in Paper I instead. However, it is expedient to obtain the solution here. The ideal resonant surface, as we have already stated, is defined by the equation $r = r_{\text{A}}$, where r_{A} is, in turn, defined by

$$\tilde{\Omega}_r^2(r_{\text{A}}) = \varpi_{\text{A}}^2(r_{\text{A}}). \quad (68)$$

Following Paper I, we make the variable substitution $s = r - r_{\text{A}}$. Equations describing the motion in the dissipative layer were derived in Paper I. When deriving these equations, the authors

approximated all coefficient functions in the equations by the first non-zero terms of their Taylor expansions with respect to s . In particular, they obtained $\tilde{\Omega}^2(r_A) - \varpi_A^2(r_A) \propto s$. However, Ruderman, Tirry & Goossens (1995) showed that, in the case of a very weak dissipation, one needs to also take the imaginary part of $\tilde{\Omega}$ into account. Hence, we use the approximate expression

$$\tilde{\Omega}^2 - \varpi_A^2 = s\Delta + 2i\varpi_i\tilde{\Omega}_r(r_A), \quad (69)$$

where ϖ_i is the imaginary part of ϖ and

$$\Delta = \frac{d}{dr}(\tilde{\Omega}^2 - \varpi_A^2) \Big|_{r=r_A}. \quad (70)$$

Now, using the equations derived in Paper I, we obtain that the equations describing the plasma motion in the dissipative layer in the cold plasma approximation read

$$\left[s\Delta + 2i\varpi_i\tilde{\Omega}_{rA} - i\tilde{\nu}\tilde{\Omega}_{rA} \frac{d^2}{ds^2} \right] \frac{d\xi_r}{ds} = \frac{\tilde{P} - 2m\tilde{T}_A\xi_r}{\rho_A r_A^2}, \quad (71)$$

$$\left[s\Delta + 2i\varpi_i\tilde{\Omega}_{rA} - i\tilde{\nu}\tilde{\Omega}_{rA} \frac{d^2}{ds^2} \right] \frac{d\tilde{P}}{ds} = \frac{2\tilde{T}_A}{\rho_A r_A^2} (\tilde{P} - 2m\tilde{T}_A\xi_r), \quad (72)$$

where $\tilde{\nu} = \epsilon^{-1}\nu$ is the scaled coefficient of viscosity, and the subscript A indicates that a quantity is calculated at $r = r_A$. Following Sakurai, Goossens & Hollweg (1991), we introduce the characteristic spatial scale δ_A in the dissipative layer and the dimensionless variable τ ,

$$\tau = \frac{s}{\delta_A}, \quad \delta_A = \left| \frac{\tilde{\nu}\tilde{\Omega}_{rA}}{\Delta} \right|^{1/3}. \quad (73)$$

Using the dimensionless variable, after some algebra, we reduce equations (71) and (72) to

$$\left(\frac{d^2}{d\tau^2} + \Lambda + i\chi\tau \right) \frac{d\xi_r}{d\tau} = \frac{i\chi(\tilde{P} - 2\tilde{T}_A\xi_r)}{\rho_A r_A^2 \Delta}, \quad (74)$$

$$\left(\frac{d^2}{d\tau^2} + \Lambda + i\chi\tau \right) \frac{d}{d\tau}(\tilde{P} - 2\tilde{T}_A\xi_r) = 0, \quad (75)$$

where

$$\Lambda = -\frac{2\varpi_i|\tilde{\Omega}_{rA}|}{\delta_A|\Delta|}, \quad \chi = \text{sgn}(\Delta\tilde{\Omega}_{rA}). \quad (76)$$

The solution to the system of equations (74) and (75) was obtained by Tirry & Goossens (1996). This solution is expressed in terms of functions $F_\Lambda(\tau)$ and $G_\Lambda(\tau)$ introduced by Goossens et al. (2011):

$$\tilde{P} - 2m\tilde{T}_A\xi_r = C_A = \text{constant}, \quad (77)$$

$$\frac{d\xi_r}{d\tau} = -\frac{i\chi C_A}{\rho_A r_A^2 \Delta} F_\Lambda(\tau), \quad \xi_r = -\frac{C_A}{\rho_A r_A^2 \Delta} G_\Lambda(\tau) + C_\xi, \quad (78)$$

where C_ξ is a constant and

$$F_\Lambda(\tau) = \int_0^\infty \exp(i\chi u\tau - u^3/3 + \Lambda u) du, \quad (79)$$

$$G_\Lambda(\tau) = \int_0^\infty \frac{\exp(i\chi u\tau) - 1}{u} e^{-u^3/3 + \Lambda u} du. \quad (80)$$

We note that the expression for $G_\Lambda(\tau)$ is slightly different from that given by Goossens et al. (2011). However, the two expressions are different by a constant. Since ξ_r is defined with the accuracy up to an additive constant, this difference does not affect it.

When a propagating wave damps ($\varpi_i < 0$), we have $\Lambda > 0$. If, in addition, Λ is large then functions $F_\Lambda(\tau)$ and $G_\Lambda(\tau)$ are strongly oscillatory. It is shown in Goossens et al. (2011) that the thickness of the dissipative layer is of the order of $lR|\omega_i|/\omega_A$, and

the maximum value of $F_\Lambda(\tau)$ in the dissipative layer is of the order of $\exp(2\Lambda^2/3)$. In addition to the thickness of the dissipative layer, there is the second, much smaller, characteristic scale. This is the characteristic wavelength of oscillations in the dissipative layer equal to $\delta_A|\Lambda|^{-1/2}$.

When a propagating wave grows ($\varpi_i > 0$), we have $\Lambda < 0$. It is shown in Appendix A that, in this case, we easily obtain that

$$F_\Lambda(\tau) = -\frac{1}{\Lambda + i\chi\tau} + \mathcal{O}(1/\Lambda^2), \quad (81)$$

$$G_\Lambda(\tau) = -\ln\left(1 + \frac{i\chi\tau}{\Lambda}\right) + \mathcal{O}(1/|\Lambda|^3). \quad (82)$$

It follows from this result that, in the leading-order approximation with respect to $1/|\Lambda|$, the real and imaginary parts of $G_\Lambda(\tau)$ are given by

$$\Re(G_\Lambda) = -\frac{1}{2} \ln\left(1 + \frac{\tau^2}{\Lambda^2}\right), \quad \Im(G_\Lambda) = -\chi \arctan \frac{\tau}{\Lambda}. \quad (83)$$

We see that the thickness of the dissipative layer is of the order of $\delta_A\Lambda \sim lR|\omega_i|/\omega_A$, that is the same as in the case of damped waves. However, there are no oscillations in the dissipative layer and, thus, there is no second characteristic scale. Now, we can specify the condition that r is not too close to r_A as imposed in the previous subsection. This condition means that $|r - r_A| > lR|\omega_i|/\omega_A$, i.e. r must be outside of the dissipative layer.

Returning to the general case, we define the jump of a quantity across the dissipative layer as

$$[f(\tau)] = \lim_{\tau \rightarrow \infty} [f(\tau) - f(-\tau)]. \quad (84)$$

To calculate $[G_\Lambda(\tau)]$ in the case where $\Lambda > 0$, we use the variable substitution $u' = u\tau$ and then drop the prime. As a result, we obtain

$$\begin{aligned} [G_\Lambda(\tau)] &= 2i\chi \lim_{\tau \rightarrow \infty} \int_0^\infty \frac{\sin(u\tau)}{u} e^{-u^3/3 + \Lambda u} du \\ &= 2i\chi \lim_{\tau \rightarrow \infty} \int_0^\infty \frac{\sin u}{u} e^{-u^3/3\tau^3 + \Lambda u/\tau} du = i\chi\pi. \end{aligned} \quad (85)$$

Using this result and equations (77) and (78), we have that

$$[\xi_r] = -\frac{i\chi\pi C_A}{\rho_A r_A^2 \Delta}, \quad [\tilde{P}] = -\frac{2im\chi\pi\tilde{T}_A C_A}{\rho_A r_A^2 \Delta}. \quad (86)$$

These expressions are called the connection formulae. They were first introduced by Sakurai et al. (1991) in the case where $\Lambda = 0$ (see also Goossens, Ruderman & Hollweg 1995; Erdélyi 1997). Later, the connection formulae were derived by Ruderman et al. (1995) in the case where $\Lambda > 0$. They showed that the connection formulae are independent of Λ . This result was later confirmed by Tirry & Goossens (1996) and Goossens et al. (2011). Here, we extended this result to the case where $\Lambda < 0$. Using equation (83), it is straightforward to show that equation (86) remains valid also in the case where $\Lambda < 0$.

3.3.3 Calculation of $[\xi_r]$ and $[\tilde{P}]$ using the ideal solution

In the theory of asymptotic methods, the solution to the ideal MHD equations far from the resonant surface is called the external solution, while the solution to the dissipative MHD equations near the resonant surface is called the internal solution (e.g. Bender & Orszag 1999). Equation (84) defines the jump of function $f(\tau)$

from the point of view of the internal solution. Using equation (73), we can also consider f as a function of s and define the jump of this function from the point of view of external solution as

$$[f(s)] = \lim_{s \rightarrow +0} [f(s) - f(-s)]. \quad (87)$$

The two expressions for the jump of f , one given by this equation and the other given by equation (84), must coincide. Using equations (60), (62), (66), and (67) to calculate $[\xi_r]$ and $[\tilde{P}]$ yields

$$[\xi_r] = \frac{\psi}{R^2(1+l)} - \eta - \frac{\eta}{R} \mathcal{P} \int_{R(1-l/2)}^{R(1+l/2)} \frac{X dr'}{\rho_t(\tilde{\Omega}_r^2 - \varpi_A^2)}, \quad (88)$$

$$[\tilde{P}] = -\eta \rho_i R(1-l/2) [(\varpi - \kappa U_0)^2 - \kappa^2 V_{Ai}^2] - \frac{\psi \rho_e (\varpi^2 - \varpi_{Ae}^2)}{R(1+l/2)} - \eta \mathcal{P} \int_{R(1-l/2)}^{R(1+l/2)} \left(\rho_t (\tilde{\Omega}^2 - \varpi_A^2) + \frac{Y(r) + \Psi(r_A)X(r)}{\rho_t(\tilde{\Omega}_r^2 - \varpi_A^2)} \right) dr, \quad (89)$$

where \mathcal{P} indicates the principal Cauchy part of integral.

3.4 Matching solutions

We now can match the expressions for $[\xi_r]$ and $[\tilde{P}]$ calculated using the dissipative and ideal solutions. To do this, we compare the expressions for the jumps of ξ_r and \tilde{P} across the dissipative layer given by equation (86), and by equations (88) and (89). As a result, we obtain

$$\frac{\psi(1-l)}{R^2} = \eta - \frac{i\chi\pi C_A}{\rho_A r_A^2 \Delta} + \frac{\eta}{R} \mathcal{P} \int_{R(1-l/2)}^{R(1+l/2)} \frac{X dr'}{\rho_t(\tilde{\Omega}_r^2 - \varpi_A^2)}, \quad (90)$$

$$\frac{\psi \rho_e (\varpi^2 - \varpi_{Ae}^2)}{R(1+l/2)} = -\eta \rho_i R(1-l/2) [(\varpi - \kappa U_0)^2 - \kappa^2 V_{Ai}^2] + \frac{2im\chi\pi\tilde{T}_A C_A}{\rho_A r_A^2 \Delta} - \eta \mathcal{P} \int_{R(1-l/2)}^{R(1+l/2)} \left(\rho_t (\tilde{\Omega}^2 - \varpi_A^2) + \frac{Y(r) + \Psi(r_A)X(r)}{\rho_t(\tilde{\Omega}_r^2 - \varpi_A^2)} \right) dr. \quad (91)$$

We now need to find the expression for C_A . Both ξ_r and \tilde{P} have a logarithmic singularity at $r = r_A$. However, it is shown in Paper I that $\tilde{P} - 2m\tilde{T}_A \xi_r$ is regular at $r = r_A$, which implies that we can use equations (60) and (66) (or equations 62 and 67) to calculate C_A . It follows from equation (70) that Δ is of the order of l^{-1} . This implies that in equations (90) and (91), C_A is multiplied by terms of the order of l . Hence, we can calculate C_A in the leading-order approximation with respect to l . Consequently, we can neglect the integral terms in equations (60) and (66) which are of the order of l , and substitute η for ξ_r . We obtain, as a result, that $C_A = \eta C_\eta$, where

$$C_\eta = \rho_i R [(\varpi - \kappa U_0)^2 - \kappa^2 V_{Ai}^2] + R \Psi_A - 2m\tilde{T}_A. \quad (92)$$

We recall that the subscript A indicates that a quantity is calculated at $r = r_A$. Substituting the expression for C_A in equations (90) and (91), we obtain the system of two linear homogeneous algebraic equations for the variables η and ψ . This system has non-trivial solutions only when its determinant is zero. This condition gives

the dispersion equation determining the dependence of ϖ on κ :

$$\begin{aligned} \rho_i [(\varpi - \kappa U_0)^2 - \kappa^2 V_{Ai}^2] + \rho_e (1+l) (\varpi^2 - \varpi_{Ae}^2) \\ = \frac{i\chi\pi C_\eta [\rho_e R (\varpi^2 - \varpi_{Ae}^2) + 2m\tilde{T}_A]}{\rho_A R^3 \Delta} \\ - \mathcal{P} \int_{R(1-l/2)}^{R(1+l/2)} \left(\frac{\rho_t}{R} (\tilde{\Omega}_r^2 - \varpi_A^2) + \frac{Y(r) + X(r) [\Psi_A + \rho_e (\varpi^2 - \varpi_{Ae}^2)]}{\rho_t R (\tilde{\Omega}_r^2 - \varpi_A^2)} \right) dr. \end{aligned} \quad (93)$$

When deriving this equation, we only kept terms of the order of unity and l , while we neglected terms of higher order with respect to l . In particular, we used the approximate relation $r_A \approx R$.

4 EVALUATION OF THE DISPERSION EQUATION

We look for the solution to the dispersion equation (93) in the form of expansion with respect to the small parameter l ,

$$\varpi = \varpi_1 + l\varpi_2 + \dots \quad (94)$$

We take into account that Δ is proportional to l^{-1} and the integrals in equation (93) are proportional to l .

4.1 First-order approximation

Collecting terms of the order of unity in equation (93) and using equation (92), we obtain

$$\rho_e (\varpi_1^2 - \varpi_{Ae}^2) + \rho_i \left[(\varpi_1 - \kappa U_0)^2 - \frac{\kappa^2 B_0^2}{\mu_0 \rho_i} \right] = 0. \quad (95)$$

We see that only the effect of axial flow is present in this equation, while the effect of the azimuthal magnetic field and flow is not. Previously, a similar result was obtained by Ruderman (2007) in the case of a twisted tube without a background flow. It is important to emphasize that this result is obtained under the assumption that the azimuthal component of the magnetic field is proportional to r , and the flow velocity is parallel to the magnetic field. Terradas & Goossens (2012) considered kink oscillations of a twisted magnetic tube with the azimuthal component of the magnetic field not proportional to r . They showed that, in this case, the wave frequency is affected by the azimuthal component of the magnetic field.

We note that equation (95) is invariant with respect to the change of sign of A . Hence, below, we assume that $A > 0$. We introduce the dimensionless quantities

$$K = \frac{kB_0}{A}, \quad \sigma = \frac{\omega_1 \sqrt{\mu_0 \rho_i}}{A}, \quad (96)$$

where $\omega_1 = \epsilon \varpi_1$, and ζ is defined by equation (29). Below, we assume that $\zeta \geq 2$. Using equations (10), (36), and (96), we transform equation (95) to

$$\zeta [(\sigma - K M_A)^2 - 2K^2] + \sigma^2 = 0, \quad (97)$$

where M_A is defined by equation (29). Equation (97) has real roots when

$$M_A < \sqrt{2(\zeta + 1)}, \quad (98)$$

and complex otherwise. The presence of complex roots corresponds to the onset of the KH instability. Below, we assume that the

inequality equation (98) is satisfied. In that case, the roots of equation (97) are

$$\sigma = \sigma_{\pm} \equiv K \frac{\zeta M_A \pm \sqrt{\zeta(2\zeta + 2 - M_A^2)}}{\zeta + 1}. \quad (99)$$

When $M_A < \sqrt{2}$, the roots have different signs. However, they are both positive when $M_A > \sqrt{2}$. Usually, in this case, the wave with the frequency σ_- is a negative energy wave (e.g. Nezhlin 1976; Ostrovskii et al. 1986; Stepanyants & Fabrikant 1989; Fabrikant & Stepanyants 1998). Below, we call the wave propagating with the dimensionless frequency σ_+ , the forward wave, and the wave propagating with the dimensionless frequency σ_- , the backward wave.

4.2 Second-order approximation

In the second-order approximation, we collect terms of the order of l in equation (93) to obtain the expression for ϖ_2 . We write it as $\varpi_2 = \varpi_{2r} - i\gamma$; ϖ_{2r} only gives small correction to the wave frequency, while γ determines the rate of wave damping (when $\gamma > 0$) or amplification (when $\gamma < 0$). Hence, below we only calculate γ . Using equation (95), we obtain

$$\gamma = \frac{\chi\pi[\rho_e R(\varpi_1^2 - \varpi_{Ae}^2) + 2m\tilde{T}_A]}{2l\rho_A R^3 \Delta[\varpi_1(\rho_i + \rho_e) - \rho_i \kappa U_0]} \times [\rho_e R(\varpi_1^2 - \varpi_{Ae}^2) + 2m\tilde{T}_A - R\Psi_A]. \quad (100)$$

This expression is used later to evaluate γ for a particular equilibrium.

5 CALCULATION OF DECREMENT FOR PARTICULAR EQUILIBRIUM

We now calculate γ for a particular equilibrium. We consider the equilibrium described in Section 3 and take $\theta \rightarrow 0$. In Section 2, we assumed that the velocity and magnetic field are continuous at the transitional layer boundaries. When $\theta \rightarrow 0$, its internal boundary becomes a tangential discontinuity. However, analysis of the derivation of the dispersion equation shows that, in fact the condition that the velocity and magnetic field are continuous at the transitional layer boundaries was not used. The only condition that we used is that ξ_r and \hat{P} are continuous at these boundaries. The continuity of these quantities at the internal boundary follows from the kinematic and dynamic boundary conditions at a tangential discontinuity.

Taking $\theta \rightarrow 0$, we obtain the equilibrium where the velocity and magnetic twist are confined in the tube core region. Since there is no background bulk flow in the transitional layer, there is no Doppler shift of the Alfvén continuum \mathfrak{A} , which is defined by

$$\mathfrak{A} = \mathfrak{A}_- \cup \mathfrak{A}_+, \quad \mathfrak{A}_- = [-\varpi_{Ae}, -\varpi_{Ai}], \quad \mathfrak{A}_+ = [\varpi_{Ai}, \varpi_{Ae}]. \quad (101)$$

The position of the resonant surface is defined by the equation $\varpi_A^2(r_A) = \varpi^2$, where we took into account that $\tilde{\Omega} = \varpi$ in the transitional layer. This equation can be rewritten in the dimensionless variables as

$$\zeta K^2 = \sigma^2 [1 + (\zeta - 1)y], \quad (102)$$

where

$$y = \frac{(2+l)R - 2r_A}{2lR}. \quad (103)$$

Using equation (99), we obtain

$$y = y_{\pm} \equiv \frac{\zeta^2 - 1 - (\zeta - 1)M_A^2 \mp 2M_A S}{(\zeta - 1)[2(\zeta + 1) + (\zeta - 1)M_A^2 \pm 2M_A S]}. \quad (104)$$

where

$$S = \sqrt{\zeta(2\zeta + 2 - M_A^2)}, \quad (105)$$

and the upper and lower signs correspond to $\sigma = \sigma_+$ and $\sigma = \sigma_-$, respectively. The condition that r_A is inside the transitional layer reduces to $0 < y < 1$. It is straightforward to show that $0 < y_+ < 1$ when

$$M_A < \sqrt{\zeta} - 1, \quad (106)$$

and $0 < y_- < 1$ when

$$M_A < \sqrt{2 - 1/\zeta} - 1 \text{ or } \sqrt{2 - 1/\zeta} + 1 < M_A < \sqrt{\zeta} + 1. \quad (107)$$

When equation (106) is satisfied, the frequency of the forward wave is in \mathfrak{A}_+ . However, when the background flow is so strong that equation (106) is not satisfied, this frequency is larger than ϖ_{Ae} , it is out of the Alfvén continuum, and the wave propagates without damping. This is in a drastic contrast with the wave behaviour in the absence of flow when the waves always damp due to resonant absorption. However, in fact, the statement that the wave propagates without damping when equation (106) is not satisfied is not completely correct. There is no wave damping caused by resonant absorption. But, since the wave frequency is larger than ϖ_{Ae} , the wave is leaky. Hence, it damps due to the energy leakage. In this case, the decrement is of the order of ϵ and, hence, it is very small in the thin tube approximation.

Now, we proceed to studying the backward wave. When the left inequality in equation (107) is satisfied, the frequency of the backward wave is in \mathfrak{A}_- and it damps due to resonance absorption. For stronger flow with the Mach number satisfying

$$\sqrt{2 - 1/\zeta} - 1 < M_A < \sqrt{2 - 1/\zeta} + 1,$$

the backward wave frequency is in the interval $(-\varpi_{Ai}, \varpi_{Ai})$, meaning that it is out of the Alfvén continuum. As a result, the backward wave propagates without damping or amplification. When the background flow speed increases further and M_A satisfies the right inequality in equation (107), the backward wave frequency is in \mathfrak{A}_+ , and the wave is affected by the resonant absorption. However, since now the wave propagates in the flow direction in the reference frame where the external plasma is at rest, it follows from the general theory that it is a negative energy wave. Hence, we can expect that the decrease in its energy caused by resonant absorption should result in the wave amplification. This result will be confirmed later by the direct calculation of γ . Finally, when the flow is so strong that $M_A > \sqrt{\zeta} + 1$, the backward wave frequency is larger than ϖ_{Ae} , that is not in the Alfvén continuum. Hence, the wave propagates without either damping or amplification caused by resonant absorption. Again, since the wave frequency is larger than ϖ_{Ae} , it is leaky. Since it is a negative energy wave, the energy leakage can cause the wave amplification. But the increment is of the order of ϵ and, consequently, it is very small in the thin tube approximation.

Let us now calculate γ . With the aid of equations (96) and (103), we obtain from equation (70)

$$\Delta = -\frac{\zeta(\zeta - 1)A^2 K^2}{\mu_0 \rho_i l R [1 + y(\zeta - 1)]^2}. \quad (108)$$

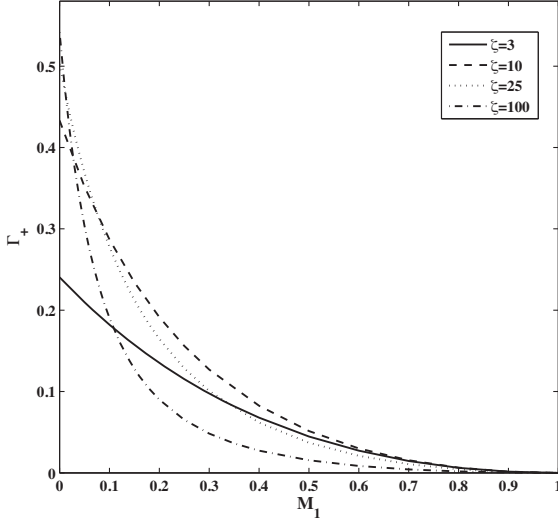


Figure 5. Dependence of Γ_+ on M_1 . The solid, dashed, dotted, and dash-dotted curves correspond to $\zeta = 3, 10, 25,$ and 100 , respectively.

Since $\Delta < 0$, it follows that $\chi = -\text{sgn}(\sigma)$. Using this result and equations (96), (103), and (108), we transform equation (100) to

$$\Gamma = \frac{\gamma \sqrt{\mu_0 \rho_i}}{AK} \equiv \frac{\pi \text{sgn}(\sigma)(a^2 - \zeta)^2 [1 + x(\zeta - 1)]}{2\zeta(\zeta - 1)[(\zeta + 1)a - \zeta M_A]}, \quad (109)$$

where $a = \sigma/K$. This expression is valid for $\sigma = \sigma_+$ when equation (106) is satisfied, and for $\sigma = \sigma_-$ when equation (107) is satisfied. Since $\sigma_+ > 0$ and $(\zeta + 1)a_+ - \zeta M_A > 0$, it follows that $\Gamma_+ > 0$ and the forward wave damps due to resonant absorption when M_A satisfies equation (106). When M_A satisfies the left inequality in equation (107), $\sigma_- < 0$ and $(\zeta + 1)a_- - \zeta M_A < 0$, so $\Gamma_- > 0$ and the backward wave also damps. Finally, when M_A satisfies the right inequality in equation (107), the backward wave propagates in the positive z -direction, $\sigma_- > 0$, $(\zeta + 1)a_- - \zeta M_A < 0$, and $\Gamma_- < 0$ meaning that the wave is subjected to resonant instability and its amplitude increases.

We calculated the decrement/increment of propagating kink waves numerically using equation (109). Fig. 5 shows the dependence of the decrement of forward kink waves, Γ_+ , on $M_1 = M_A/(\sqrt{\zeta} - 1)$ for various values of ζ . We see that the presence of flow reduces the efficiency of resonant damping, and the waves propagate without resonant damping for $M_1 > 1$.

Fig. 6 displays the dependence of the decrement of backward kink waves, Γ_- , on $M_2 = M_A/(\sqrt{2 - 1/\zeta} - 1)$ for various values of ζ . We see that the larger ζ is the stronger the damping. The presence of flow reduces the efficiency of resonant damping for $\zeta = 3$, but increases it for larger values of ζ . The waves propagate without resonant damping for $M_2 > 1$.

Fig. 7 shows the dependence of Γ_- on $M_3 = M_A/(\sqrt{\zeta} + 1)$ for various values of ζ . We see that in this figure $\Gamma_- < 0$, which indicates that in this case there is the resonant instability with the increment equal to $|\Gamma_-|$. In accordance with the right inequality in equation (107), the dependence of Γ_- on M_3 is shown for $M_3 \in [\sqrt{2 - 1/\zeta} + 1, 1]$. An interesting feature of the resonant instability is that its increment is a decreasing function of the flow magnitude. When $M_3 > 1$, the wave propagates without growth.

We need to make a comment about the dependence of Γ on M_A . When $M_2 > 1$, then $\Gamma_- = 0$ implying that $\Gamma_- \rightarrow 0$ as $M_2 \rightarrow 1 + 0$, that is M_2 tends to 1 from the right. On the other hand, we see in Fig. 6 that Γ_- tends to a non-zero value as $M_2 \rightarrow 1 - 0$, that is M_2

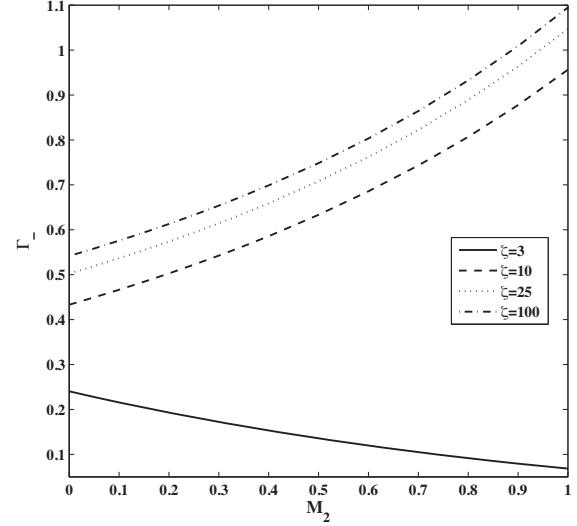


Figure 6. Dependence of Γ_- on M_2 . The solid, dashed, dotted, and dash-dotted curves correspond to $\zeta = 3, 10, 25,$ and 100 , respectively.

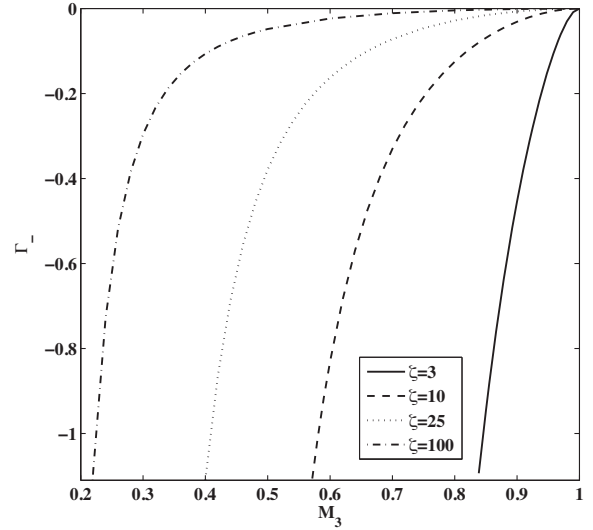


Figure 7. Dependence of Γ_- on M_3 . The solid, dashed, dotted, and dash-dotted curves correspond to $\zeta = 3, 10, 25,$ and 100 , respectively.

tends to 1 from the left. Hence, $\Gamma_- = 0$ is discontinuous at $M_2 = 1$. This feature is the direct consequence of the equilibrium model with the discontinuity at the internal boundary of the transitional layer. If we consider a model not with $\theta \rightarrow 0$ but with finite $\theta \ll 1$, then Γ_- would drop from a finite value to zero in a small interval with the length of the order of θl near $M_2 = 1$. The same analysis refers to Fig. 7. Γ_- is discontinuous at $M_3 = \sqrt{2 - 1/\zeta} + 1$, being equal to zero at the left of this point and non-zero at the right. Again, if we consider a model with finite $\theta \ll 1$ then Γ_- would drop from a finite value to zero in a small interval with the length of the order of θl near $M_3 = \sqrt{2 - 1/\zeta} + 1$.

6 APPLICATION TO SPICULES AND FILAMENTS IN THE SOLAR ATMOSPHERE

In this section, we apply the theoretical results to observation of waves in spicules in the solar atmosphere. Propagating kink waves,

as we have already stated, were observed in spicules (e.g. De Pontieu et al. 2007; He et al. 2009a,b). One possible mechanism of generation of these waves is instability. The presence of flow can cause the KH instability. This type of instability in spicules was studied by a few authors. Zhelyazkov & Zaqarashvili (2012) modelled a type II spicule as a magnetic tube with the straight magnetic field inside and outside and the flow inside the tube using typical values of spicule parameters. In particular, they took $\zeta = 100$. They only considered the tube stability with respect to the sausage and kink modes. The main conclusions made by these authors are as follows. The sausage waves are stable for any flow magnitude, while the kink waves become unstable for sufficiently large velocity magnitude. However, this instability only occurs when $M_A \gtrsim 10$, which corresponds to the flow magnitude greatly exceeding the observed values. Using equations (98) and (107), we obtain that the ratio of the critical velocity for the onset of the KH instability to that for the onset of the resonant instability is

$$\Theta = \frac{\sqrt{2(\zeta + 1)}}{\sqrt{2 - 1/\zeta + 1}}. \quad (110)$$

For $\zeta = 100$, we obtain $\Theta \approx 6$. Hence, for the same values of parameters that were taken by Zhelyazkov & Zaqarashvili (2012), kink waves can be subject to the resonant instability for $M_A \gtrsim 2$. This is a rather realistic value not contradicting to the observations.

Zhelyazkov, Zaqarashvili & Chandra (2015) and Zhelyazkov & Chandra (2019) studied the KH instability in spicules modelling them as tubes with twisted magnetic field. They showed that the tube can be KH unstable for realistic values of spicule parameters, however, only with respect to fluting wave modes, while the kink waves remain stable. Hence, to excite the kink waves, we need to involve resonant instability.

Zhelyazkov (2015) considered the KH instability of a filament observed during an eruption on 2011 February 24 (Möstl, Temmer & Veronig 2013). To model this instability, Zhelyazkov took $\zeta \gtrsim 10$, the Alfvén speed inside the tube equal to 226 km s^{-1} , and the flow speed inside the tube equal to 310 km s^{-1} . He showed that the tube is unstable with respect to the fluting mode with the azimuthal number $m = -3$. However, the kink mode becomes unstable only for the flow speed equal to 1140 km s^{-1} , which strongly exceeds the observed value. For $\zeta = 10$, we obtain $\Theta \approx 2$, so the kink wave is subject to resonant instability for the flow velocity equal to 570 km s^{-1} , which is much closer to the observed value, but still too high. However, the value of ζ is not well known. If we take $\zeta = 40$, then $\Theta \approx 3.75$ and the kink mode becomes resonantly unstable for the flow speed approximately equal to 300 km s^{-1} , which is smaller than the observed value.

7 SUMMARY AND CONCLUSIONS

In this article, we studied propagating kink waves in a twisted tube in the presence of flow. The tube consists of a core region and a transitional or boundary layer. There is no flow and magnetic twist outside the tube. We assumed that the flow velocity is parallel to the magnetic field lines. The plasma density is constant inside and outside the tube, and it decreases monotonically in the transitional layer from its value inside the tube to that outside the tube. The background flow speed and magnetic twist monotonically decrease from their values in the core region of the tube to zero in the transitional layer. Using the TTTB approximation, we derived the dispersion equation determining the dependence of the wave frequency and decrement/increment on the wavenumber.

Two important parameters determining the properties of kink waves are the ratio of densities inside and outside the tube ζ and the Alfvén Mach number M_A equal to the ratio of the flow speed to the Alfvén speed in the tube core region. When M_A exceeds the KH threshold equal to $\sqrt{2(\zeta + 1)}$, the kink wave is subjected to KH instability. We assumed that $M_A < \sqrt{2(\zeta + 1)}$, so the kink waves are KH stable.

The density and magnetic field variation in the transitional layer results in the existence of Alfvén continuum. When the kink wave frequency is in the Doppler-shifted Alfvén continuum, this wave is subjected either to resonant damping or to resonant instability. We studied the properties of kink waves in a particular unperturbed state, where there is no background flow and magnetic twist in the transitional layer. Kink waves propagating in a static magnetic tube are always damp due to resonant absorption. However, the background flow can swipe the kink wave frequency out of the Alfvén continuum. For a kink wave propagating in the flow direction this occurs when $M_A > \sqrt{\zeta} - 1$. In this case, the wave propagates without resonant damping in spite of the existence of the Alfvén continuum. The frequency of a kink wave propagating in the direction opposite to that of the flow is out of the Alfvén continuum when $\sqrt{2 - 1/\zeta} - 1 < M_A < \sqrt{2 - 1/\zeta} + 1$, so this wave propagates without resonant damping.

When $M_A > \sqrt{2}$, the kink wave propagating in the direction opposite to that of the background flow in the reference frame moving together with the flowing plasma starts to propagate in the flow direction in the reference frame where the plasma outside the tube is at rest. In accordance with the general theory, it becomes a negative energy wave and can be unstable if there is any mechanism decreasing its energy. Since we assume that the plasma is very weakly dissipative, the only mechanism that can decrease the wave energy is resonant absorption. However, it is only possible when the wave frequency is in the Alfvén continuum. If this is the case, then the wave is resonantly unstable. To satisfy the condition that the wave frequency is in the Alfvén continuum one needs M_A slightly larger than $\sqrt{2}$, namely, $M_A > \sqrt{2 - 1/\zeta} + 1$. The quantity $\sqrt{2 - 1/\zeta} + 1$ is the resonant instability threshold. An important property is that this threshold is lower than the KH instability threshold for any $\zeta > 1$. Moreover, for large ζ , the ratio of the KH threshold to the resonant instability threshold is large. For example, it is larger than 6 when $\zeta = 100$, which is the typical value for spicules.

The theoretical results were applied to the problem of excitation of propagating kink waves in spicules and filaments frequently observed in the solar atmosphere. We found that, for typical parameters of spicules, kink waves can be subject to resonant instability when the flow speed in a spicule exceeds 300 km s^{-1} . This instability can also excite kink waves in filaments if $\zeta \gtrsim 40$.

ACKNOWLEDGEMENTS

MSR and NSP gratefully acknowledge financial support from the Russian Fund for Fundamental Research (RFFR) grant (19-02-00111)

REFERENCES

- Andries J., Goossens M., 2001, *A&A*, 368, 1083
 Andries J., van Doorsselaere T., Roberts B., Verth G., Verwichte E., Erdélyi R., 2001, *Space Sci. Rev.*, 149, 3
 Arregui I., 2018, *Living Rev. Sol. Phys.*, 15, 3

- Aschwanden M. J., Fletcher L., Schrijver C. J., Alexander D., 1999, *ApJ*, 520, 880
- Bahari K., 2017, *Sol. Phys.*, 292, 10
- Bahari K., 2018, *ApJ*, 864, 2
- Bahari K., Khalvandi M. R., 2017, *Sol. Phys.*, 292, 11
- Bender C. M., Orszag S. A., 1999, *Advanced Mathematical Methods for Scientists and Engineers*, McGraw-Hill, New York
- Bennett K., Roberts B., Narain U., 1999, *Sol. Phys.*, 185, 41
- Brekke P., Kjeldseth-Moe O., Harrison R. A., 1997, *Sol. Phys.*, 175, 511
- Carter B. K., Erdélyi R., 2007, *A&A*, 475, 323
- Carter B. K., Erdélyi R., 2008, *A&A*, 481, 239
- Chae J., Ahn K., Lim E.-K., Choe G. S., Sakurai T., 2008, *ApJ*, 689, L73
- Cheremnykh O., Fedun V., Ladikov-Roev Yu., Verth G., 2018, *ApJ*, 866, 86
- Cirtain J. W. et al., 2007, *Science*, 318, 1580
- De Pontieu B. et al., 2007, *Science*, 318, 1574
- Doyle J. G., Taroyan Y., Ishak B., Madjarska M. S., Bradshaw S. J., 2006, *A&A*, 452, 1075
- Ebrahimi Z., Bahari K., 2019, *MNRAS*, 490, 1644
- Erdélyi R., 1997, *Sol. Phys.*, 171, 49
- Erdélyi R., Fedun V., 2010, *Sol. Phys.*, 263, 63
- Erdélyi R., Taroyan Y., 2003, *J. Geophys. Res.*, 108, 1043
- Fabrikant A. L., Stepanyants Yu. A., 1998, *Series on Nonlinear Science Series A Vol. 18, Propagation of Waves in Shear Flows*, World Scientific Press, Singapore
- Goossens M., Ruderman M. S., 1995, *Phys. Scr.*, T60, 171
- Goossens M., Hollweg J. V., Sakurai T., 1992, *Sol. Phys.*, 138, 233
- Goossens M., Ruderman M. S., Hollweg J. V., 1995, *Sol. Phys.*, 157, 75
- Goossens M., Andries J., Aschwanden M. J., 2002, *A&A*, 394, L39
- Goossens M., Terradas J., Andries J., Arregui I., Ballester J. L., 2009, *A&A*, 503, 213
- Goossens M., Erdélyi R., Ruderman M. S., 2011, *Space Sci. Rev.*, 158, 289
- He J.-S., Marsch E., Tu C.-Y., Guo L. J., Tian H., 2009a, *ApJ*, 705, L217
- He J.-S., Tu C.-Y., Marsch E., Guo L. J., Yao S., Tian H., 2009b, *A&A*, 497, 525
- Hillier A., Morton R. J., Erdélyi R., 2013, *ApJ*, 779, L16
- Hollweg J. V., Yang G., 1988, *J. Geophys. Res.*, 93, 5423
- Ionson J. A., 1978, *ApJ*, 226, 650
- Kamio S., Curdt W., Teriaca L., Inhester B., Solanki S. K., 2010, *A&A*, 510, L1
- Karami K., Bahari K., 2012, *ApJ*, 757, 186
- Kuridze D., Morton R. J., Erdélyi R., Dorrian G. D., Mathioudakis M., Jess D. B., Keenan F. P., 2012, *ApJ*, 750, 51
- Lin Y., Engvold O., Rouppe van der Voort L. H. M., van Noort M., 2007, *Sol. Phys.*, 246, 65
- Lin Y., Solar R., Engvold O., Ballester J. L., Langangen Ø., Oliver R., Rouppe van der Voort L. H. M., 2009, *ApJ*, 704, 870
- Liu W., Berger T. E., Title A. M., Tarbell T. D., 2009, *ApJ*, 707, L37
- Liu C. et al., 2011, *ApJ*, 707, L37
- Morton R., Verth G., Jess D. B., Kuridze D., Ruderman M. S., Mathioudakis M., Erdélyi R., 2012, *Nature Commun.*, 3, 1315
- Möstl U. V., Temmer M., Veronig A. M., 2013, *ApJ*, 766, L12
- Nakariakov V. M., Ofman L., Deluca E. E., Roberts B., Davila J. M., 1999, *Science*, 285, 862
- Nezlin M. V., 1976, *Sov. Phys. Uspekhi*, 19, 946
- Nishizuka N., Nakamura T., Kawate T., Singh K. A. P., Shibata K., 2011, *ApJ*, 731, 43
- Ofman L., Wang T. J., 2008, *A&A*, 482, L9
- Okamoto T. J. et al., 2007, *Science*, 318, 1577
- Ostrovskii L. A., Rybak S. A., Tsimring L. Sh., 1986, *Sov. Phys. Uspekhi*, 29, 1040
- Pascoe D. J., Wright A. N., De Moortel I., 2010, *ApJ*, 711, 990
- Raouafi N. E. et al., 2016, *Space Sci. Rev.*, 201, 1
- Ruderman M. S., 2007, *Sol. Phys.*, 246, 119
- Ruderman M. S., 2010, *Sol. Phys.*, 267, 377
- Ruderman M. S., 2015, *A&A*, 575, A130
- Ruderman M. S., Belov N. A., 2010, *J. Phys.: Conf. Ser.*, 216, 012016
- Ruderman M. S., Erdélyi R., 2009, *Space Sci. Rev.*, 149, 199
- Ruderman M. S., Petrukhin N. S., 2019, *A&A*, 631, A31
- Ruderman M. S., Roberts B., 2002, *ApJ*, 577, 475
- Ruderman M. S., Terradas J., 2015, *A&A*, 580, A57
- Ruderman M. S., Wright A. N., 1998, *J. Geophys. Res.*, 103, 26573
- Ruderman M. S., Tirry W., Goossens M., 1995, *J. Plasma Phys.*, 54, 129
- Ryutov D. D., Ryutova M. P., 1976, *Sov. Phys. JETP*, 43, 491
- Ryutova M. P., 1988, *Sov. Phys. JETP*, 67, 1594
- Sakurai T., Goossens M., Hollweg J. V., 1991, *Sol. Phys.*, 133, 227
- Shibata K. et al., 2007, *Science*, 318, 1591
- Shukhobodskiy A. A., Ruderman M. S., 2018, *A&A*, 615, A156
- Soler R., Goossens M., 2011, *A&A*, 531, A167
- Stepanyants Yu. A., Fabrikant A. L., 1989, *Sov. Phys. Uspekhi*, 32, 783
- Taroyan Y., Ruderman M. S., 2011, *Space Sci. Rev.*, 158, 505
- Teriaca L., Banerjee D., Falchi A., Doyle J. G., Madjarska M. S., 2004, *A&A*, 427, 1065
- Terra-Homem M., Erdélyi R., Ballai I., 2003, *Sol. Phys.*, 217, 199
- Terradas J., Goossens M., 2012, *A&A*, 548, A112
- Terradas J., Arregui I., Oliver R., Ballester J. L., 2008, *ApJ*, 678, L153
- Terradas J., Arregui I., Oliver R., Ballester J. L., 2011, *ApJ*, 729, L22
- Tian H., Curdt W., Marsch E., He J., 2008, *ApJ*, 681, L121
- Tian H., Marsch E., Curdt W., He J., 2009, *ApJ*, 704, 883
- Tirry W. J., Goossens M., 1996, *ApJ*, 471, 501
- Tirry W. J., Cadez V. M., Erdélyi R., Goossens M., 1998, *A&A*, 332, 786
- Tomczyk S., McIntosh S. W., 2009, *ApJ*, 697, 1384
- Tomczyk S., McIntosh S. W., Keil S. L., Judge P. G., Schad T., Seeley D. H., Edmondson J., 2007, *Science*, 317, 1192
- Vasheghani Farahani S., Van Doorselaere T., Verwichte E., Nakariakov V. M., 2009, *A&A*, 498, L29
- Winebarger A. R., DeLuca E. E., Golub L., 2001, *ApJ*, 553, L81
- Winebarger A. R., Warren H., van Ballegoijen A., DeLuca E. E., Golub L., 2002, *ApJ*, 567, L89
- Zaqarashvili T. V., Vörös Z., Zhelyazkov I., 2014, *A&A*, 561, A62
- Zhang Q. M., Ji H. S., 2014, *A&A*, 561, A134
- Zhelyazkov I., 2015, *J. Astrophys. Astron.*, 36, 233
- Zhelyazkov I., Chandra R., 2019, *Sol. Phys.*, 294, 233
- Zhelyazkov I., Zaqarashvili T. V., 2012, *A&A*, 547, A14
- Zhelyazkov I., Zaqarashvili T. V., Chandra R., 2015, *A&A*, 574, A55

APPENDIX A: EVALUATION OF ASYMPTOTIC EXPRESSIONS

We obtain asymptotic expressions for $F_{\Lambda}(\tau)$ and $G_{\Lambda}(\tau)$ in the case where $\Lambda < 0$ and $|\Lambda| \gg 1$. First, we consider $F_{\Lambda}(\tau)$. We rewrite the expression for $F_{\Lambda}(\tau)$ as

$$F_{\Lambda}(\tau) = \int_0^{\infty} \exp(i\chi u\tau + \Lambda u) du + I(\tau), \quad (\text{A1})$$

where

$$I(\tau) = \int_0^{\infty} \exp(i\chi u\tau + \Lambda u)(e^{-u^3/3} - 1) du. \quad (\text{A2})$$

Then, we rewrite the expression for I as $I = I_1 + I_2$, where

$$I_1(\tau) = \int_0^{|\Lambda|^{-1/2}} \exp(i\chi u\tau + \Lambda u)(e^{-u^3/3} - 1) du, \quad (\text{A3})$$

$$I_2(\tau) = \int_{|\Lambda|^{-1/2}}^{\infty} \exp(i\chi u\tau + \Lambda u)(e^{-u^3/3} - 1) du. \quad (\text{A4})$$

Using the inequality

$$1 - e^{-u^3/3} < u^3/3 \quad (\text{A5})$$

valid for $u > 0$, we obtain

$$|I_1(\tau)| < \frac{1}{3} \int_0^{|\Lambda|^{-1/2}} u^3 du = \frac{1}{12\Lambda^2}. \quad (\text{A6})$$

Next, we obtain

$$|I_2(\tau)| < \int_{|\Lambda|^{-1/2}}^{\infty} e^{\Lambda u} \mathbf{d}u = \frac{1}{|\Lambda|} e^{-|\Lambda|^{1/2}}. \quad (\text{A7})$$

Using equations (A6) and (A7) and calculating the integral in equation (A1), we arrive at equation (81).

Now, we proceed to the evaluation of $G_\Lambda(\tau)$. We write $G_\Lambda(\tau) = J_1 - J_2$, where

$$J_1(\tau) = \int_0^{\infty} \frac{\exp(i\chi u \tau) - 1}{u} e^{\Lambda u} \mathbf{d}u, \quad (\text{A8})$$

$$J_2(\tau) = \int_0^{\infty} \frac{\exp(i\chi u \tau) - 1}{u} \left(1 - e^{-u^3/3}\right) e^{\Lambda u} \mathbf{d}u. \quad (\text{A9})$$

Using equation (A5), we obtain

$$J_2(\tau) < \frac{2}{3} \int_0^{\infty} u^2 e^{\Lambda u} \mathbf{d}u = \frac{4}{3|\Lambda|^3}. \quad (\text{A10})$$

Differentiating equation (A8) yields

$$\frac{\mathbf{d}J_1}{\mathbf{d}\tau} = i\chi \int_0^{\infty} \exp(i\chi u \tau + \Lambda u) \mathbf{d}u = -\frac{i\chi}{i\chi \tau + \Lambda}. \quad (\text{A11})$$

Integrating this equation and taking into account that $J_1(0) = 0$, we obtain

$$J_1(\tau) = -\ln\left(1 + \frac{i\chi \tau}{\Lambda}\right). \quad (\text{A12})$$

Using equations (A10) and (A12), we arrive at equation (82).

This paper has been typeset from a $\text{\TeX}/\text{\LaTeX}$ file prepared by the author.